Contents lists available at ScienceDirect

Chemical Engineering Science

journal homepage: www.elsevier.com

The role of initial geometry in experimental models of wound closing

Wang Jin[a], Kai-Yin Lo[b], Shih–En Chou[b], Scott W. McCue[a], Matthew J. Simpson[a, *]

[a] School of Mathematical Sciences, Queensland University of Technology (QUT), Brisbane, Queensland 4000, Australia
[b] Department of Agricultural Chemistry, National Taiwan University, Taipei 10617, Taiwan

ARTICLE INFO

Keywords:
Wound healing assay
Sticker assay
Wound shape
Transport process

ABSTRACT

Standard wound healing assays often deal with just one initial wound shape, and it is unclear whether varying the initial wound shape might impact how we interpret results from these experiments. Here, we use a new kind of wound healing assay, called a *sticker assay*, to explore the role of initial wound shape. We examine wound healing with square, circular and triangular wounds. Measurements of wound area as a function of time show that the rate of wound closure depends on the initial wound shape. This is interesting because the only aspect of the assay we change is the initial wound shape, and the reason for different closure rates is unclear. To provide more insight we calibrate a typical mathematical model to match the data. This shows that the rates of cell motility and proliferation associated with different initial wound shapes are approximately the same, implying that the differences in the closure rates are consistent with a typical mathematical model of wound healing. Therefore, parameter estimates from an experiment with a particular wound shape can be used to predict an experiment with a different initial wound shape.

1. Introduction

Two–dimensional cell migration assays are routinely used to study wound healing. In these assays, cell migration and cell proliferation play a key role (Keese et al., 2004). There are two types of cell migration assays: (1) *Proliferation assays* are initiated by placing cells as a uniform monolayer, at low density, onto a two-dimensional surface (Tremel et al., 2009); and (2) *Wound healing assays* are initiated by creating an artificial wound in a uniformly distributed monolayer of cells (Kramer et al., 2013). In a proliferation assay, cells undergo migration and proliferation events, which increases the cell density in the uniform monolayer. Wound healing assays involve individual cells moving into the initially–vacant wound area, and the combined effects of migration and proliferation leads to the closure of the wound (Kramer et al., 2013).

Various types of wound healing assays are reported in the literature. Despite the fact that real wounds can take on arbitrary shapes and sizes, the most common wound shapes used in *in vitro* wound healing assays are a simple long thin rectangular wounds or circular wounds (Keese et al., 2004; Riahi et al., 2012; Tremel et al., 2009; van der Meer et al., 2010; Yarrow et al., 2004) and the question of whether the initial wound shape plays an important role is often overlooked (see Table 1). Madison and Gronwall (1992) compare the rate of healing for circular and square skin wounds on the dorsum of the metacarpus of horses, and they suggest that the rate of wound healing is not affected by the initial wound shape. However, more recent quantitative analysis of several *in vitro* models suggest that the rate of wound healing can be extremely sensitive to the initial configuration of cells (Jin et al., 2016,; Treloar et al., 2014). Therefore, it is of interest to develop a new *in vitro* assay which can be used to study wound healing for a variety of wound shapes, and to analyze results from the new experiments using a mathematical model to provide quantitative insight into the role of initial wound shape.

Experimental data from *in vitro* wound healing assays are commonly presented by plotting the time evolution of wound area (Bachstetter et al., 2016; Johnston et al., 2015; Ueck et al., 2017; Yarrow et al., 2004). While some studies report the time evolution of the exact wound area (Leu et al., 2012; Ueck et al., 2017; Yarrow et al., 2004), others report the wound area relative to the initial wound area (Ascione et al., 2017; Bachstetter et al., 2016; Johnston et al., 2015; Katakowski et al., 2010). Although both types of measurements provide an indication of the speed at which healing takes place, reporting the data in terms of the relative wound area does not provide any information about the role of initial wound shape or initial wound

* Corresponding author.
Email address: matthew.simpson@qut.edu.au (M.J. Simpson)

https://doi.org/10.1016/j.ces.2018.01.004
Received 29 September 2017; Received in revised form 30 November 2017; Accepted 6 January 2018
Available online xxx
0009-2509/

Table 1
A summary of various types of wound healing assays.

Assay type	Wound shape	Advantages	Limitations
Scratch assay	Long, thin rectangle (Jin et al., 2016)	Straightforward to perform (Liang et al., 2007) Relatively economic (Liang et al., 2007)	Disturb surrounding cells (Jin et al., 2017) Disrupt substrate (Liang et al., 2007) Not well–defined scratch areas (Gough et al., 2011)
Barrier assay	Rectangle (Vedula et al., 2013) Circle (Treloar and Simpson, 2013)	Can vary the spreading direction (Treloar and Simpson, 2013)	May require dry substrate (Ariano et al., 2011)
Electric impedance assay	Rectangle (Mamouni and Yang, 2011) Circle (Keese et al., 2004)	Monitor wound automatically (Keese et al., 2004)	Require special plates (Keese et al., 2004)
Stamp assay	Arbitrary (Lee et al., 2010)	Arbitrary wound shapes (Lee et al., 2010) Presence of cell debris (Lee et al., 2010)	Require specific stamps (Lee et al., 2010)
Sticker assay	Arbitrary	Arbitrary wound shapes Straightforward to perform	Require laser scriber

size. Therefore, when comparing wound healing assays with different initial wound shapes, it is important to report data in terms of the wound area because this explicitly accounts for differences in the initial condition.

Many different types of mathematical and computational models have been used to mimic *in vitro* collective cell migration assays. One approach is to use a discrete random walk model. In some random walk models, cell migration is represented by an unbiased, nearest-neighbour exclusion process, in which cell-to-cell crowding is modelled by hard core exclusion (Simpson et al., 2010). Cell proliferation can be modelled by allowing individual agents in the simulation to divide to produce daughter agents (Simpson et al., 2010). Crowding effects can be incorporated into the proliferation mechanism by randomly choosing a nearest neighbour lattice site for the placement of the daughter agent, and only allowing the proliferation event to succeed if the target site is vacant (Simpson et al., 2010). While discrete random walk models provide information relevant to individual cells within the population, it is also possible to describe the behaviour of the population of cells by considering the continuum-limit description of the random walk model, which in this case, gives rise to a two-dimensional reaction diffusion partial differential equation (PDE) that is equivalent to the two-dimensional Fisher-Kolmogorov model (Fisher, 1937).

In this study describe a novel experimental approach to investigate the role of initial wound shape. We perform sticker assays using fibroblast cells and three different initial wound shapes. In addition, we quantify the mechanisms that drive the wound healing process by calibrating the solution of a typical mathematical model to match the experimental data. Overall, while we find that different initial wound shapes lead to different rates of wound closure, our calibration of a mathematical model to the experimental data confirms that the differences in observed wound closure rates are entirely consistent with the underlying transport phenomena that drive wound healing.

2. Methods

2.1. Experimental methods

The experimental protocol for the sticker assay is shown in Fig. 1. Experiments are performed with the NIH 3T3 fibroblast cell line purchased from the Bioresource Collection and Research Center (BCRC), Taiwan. Dulbecco's Modified Eagle's medium (DMEM, Gibco, USA) and 10% calf serum (CS, Invitrogen, USA) is used for cell culture. Cells are incubated in tissue culture polystyrene (TCPS) flasks (Corning, USA) in 5% CO_2 at 37 °C, and grown to approximately 90% confluence before each passage.

Wound shapes are drawn in AutoCAD (Autodesk, USA) and loaded into a CO_2 laser scriber (ILS2, Laser Tools & Technics Corp., Taiwan), to ablate the desired wound shapes on a double-sided sticker (8018, 3M, USA). Three different types of wound shapes are designed: square, circle, and equilateral triangles. The side length of each square and triangle sticker is 2 mm, and the diameter of each circle sticker is 2 mm. The sticker is folded to form a handle, and attached to the centre of a dish, with a diameter 35 mm. The dish is exposed to UV for 30 min for sterilisation. 3×10^5 cells are placed, as uniformly as possible, into the dish, and incubated overnight. To initiate the wound healing assay, the sticker is removed to reveal the cell-free wound area. The plates are continually incubated in 5% CO_2 at 37 °C. The distribution of cells is imaged at $t = 0, 9, 24, 33, 48, 57, 72$ h for the assays initiated with the square and circular wound shapes. The assays initiated with the triangular wounds are imaged at $t = 0, 9, 24, 33, 48, 57$ h. For each shape, we perform three identically prepared experiments ($n = 3$).

A proliferation assay is initiated in the same way as the wound healing assay except that there is no wound. The plates are continually incubated in 5% CO_2 at 37 °C and images are recorded at $t = 0, 9, 24, 33, 48, 57, 72, 81, 96$ h. We perform one experimental replicate of the proliferation assay and analyse the data by estimating the cell density in three different, identically–sized, rectangular subregions (Johnston et al., 2015).

2.2. Edge detection method

We use ImageJ to detect the edges of the wound area in both the experimental and the simulation images (Treloar and Simpson, 2013). For all images, the scale is set using the *Set Scale* function. We find that 932 pixels corresponds to 1 mm for all experimental images, and 304 pixels corresponds to 1 mm for all the simulation images. For each experimental image, the contrast is enhanced (*Image–Adjust–Brightness/Contrast*). Edges of cells are detected (*Plugins–Canny Edge Detector*), and enhanced using the Sobel method (*Process–Find Edges*) (Treloar and Simpson, 2013). Depending on the quality of the experimental image, the *Find Edges* function may need to be used several times, both locally and globally to detect the edge of the wound area. The edge of the wound area is automatically detected using the wand tracing tool, and the wound area is calculated (*Analyze–Measure*). For each simulation image, the colour image is first set to grayscale (*Image–Type–32-bit*). Then the edges of cells are detected (*Plugins–Canny Edge Detector*), and

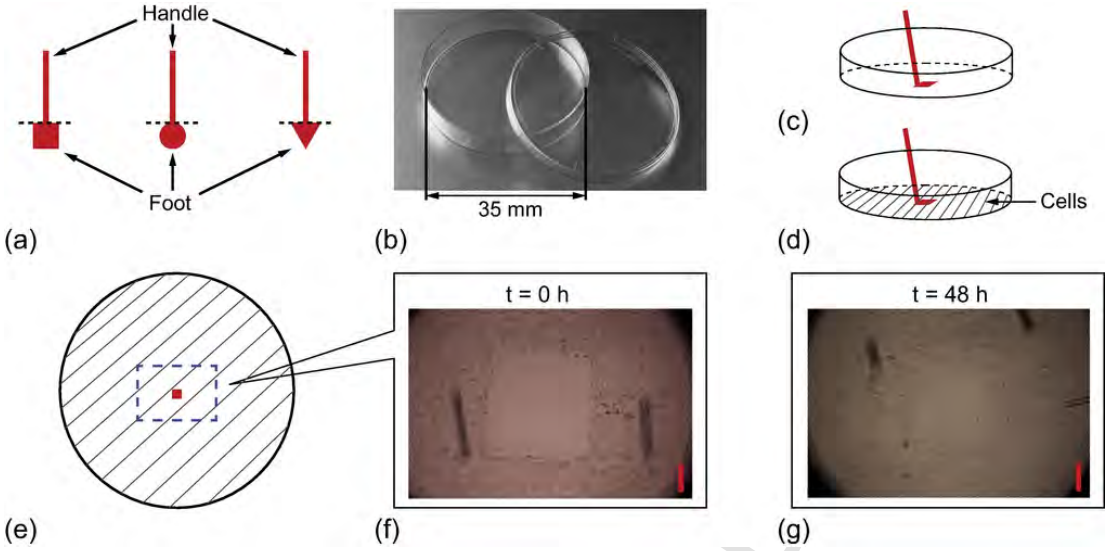

Fig. 1. Sticker assay protocol. (a) Stickers for square, circular, and triangular wound shapes. The side length and the diameter of square, equilateral triangle, and circular stickers are 2 mm. The dashed lines indicates where the sticker is folded to create the handle so that the foot of the sticker can be attached and removed from the tissue culture plate. (b) Corning® cell culture dish. (c) Schematic of a 35 mm diameter cell culture plate showing the sticker attached to the plate before the cells are seeded into the dish. (d) Schematic of the cell culture plate showing the apparatus after the cells are seeded into the dish. (e) Top view of the experiment prior to the sticker being lifted. The blue dashed area shows the field of view. (f) Experimental field of view at $t = 0$ h with a square wound shape. (g) Experimental field of view at $t = 48$ h showing the progression of the assay. The scale bar corresponds to 500 μm.

enhanced using the Sobel method (*Process–Find Edges*) two to three times. The wound area is automatically detected using the wand tracing tool and calculated (*Analyze–Measure*). An important feature of our method is that we use the exact same image processing tools to quantify the time evolution of the area of the wound in both the experimental and the simulation images.

2.3. Mathematical methods

We use a discrete model, in which each agent represents a single cell, to simulate the experiments. A hexagonal lattice, with lattice spacing taken to be equal to the cell diameter, $\Delta = 25\,\mu$m (Simpson et al., 2013), is used. Crowding effects are incorporated by ensuring that at most one agent occupies a lattice site. Potential motility or proliferation events that would place more than one agent on a site are aborted. Details of the discrete model are given in the Supplementary Material document.

The discrete model is associated with a reaction–diffusion equation in the continuum limit (Supplementary Material). The reaction–diffusion equation can be written as

$$\frac{\partial \mathscr{C}(x,y,t)}{\partial t} = D\nabla^2\mathscr{C}(x,y,t) + r\mathscr{C}(x,y,t)\left(1 - \frac{\mathscr{C}(x,y,t)}{K}\right), \tag{1}$$

where $C(x,y,t)$ [cells/μm^2] is cell density, D [μm^2/h] is the cell diffusivity, r [/h] is the proliferation rate, and K [cells/μm^2] is the carrying capacity density. When modelling proliferation assays, in which $\nabla^2\mathscr{C}(x,y,t) = 0$, the two-dimensional PDE, with independent variable $\mathscr{C}(x,y,t)$, simplifies to an ordinary differential equation (ODE) with independent variable $\mathscr{C}(t)$,

$$\frac{\mathrm{d}\mathscr{C}(t)}{\mathrm{d}t} = r\mathscr{C}(t)\left(1 - \frac{\mathscr{C}(t)}{K}\right), \tag{2}$$

where $\mathscr{C}(t)$ [cells/μm^2] is the cell density, and t [h] is time. The solution of Eq. (2) is

$$\mathscr{C}(t) = \frac{K\mathscr{C}(0)}{(K - \mathscr{C}(0))\,\mathrm{e}^{-rt} + \mathscr{C}(0)}. \tag{3}$$

2.4. Motivation

While it is obvious that real wounds take on arbitrary shapes and sizes, *in vitro* wound healing assays are almost always limited to just one particular wound shape. Therefore, the role of initial wound shape in *in vitro* experimental models is poorly understood because it has not been previously examined. An implicit assumption, that is rarely stated and never tested, is that when an *in vitro* wound healing assay with a specific initial wound shape is performed, the results could be extrapolated to apply to a different situation where a wound is created with a different shape. For example, a relevant question for us to consider is if we perform a sticker assay with a square wound, can the results from that assay be applied to predict the closure of a circular wound? This question motivates our present work in which we perform, and analyse, a series of sticker assays with a range of initial wound shapes. Using our mathematical model we calibrate values of r,K and D so that our mathematical model matches the observations from the experimental data, and we can quantitatively assess the role of wound shape by comparing parameter estimates obtained by considering experiments with different initial wound shape. We are particularly interested in this question because recent studies that combine *in vitro* wound healing assays with mathematical models show that the results of these experiments can be extremely sensitive to the initial configuration of the experiments (Jin et al., 2016,; Treloar et al., 2014).

3. Results and discussion

3.1. Estimating the rate of wound closure

We use the edge detection method to locate the leading edge of the wound and to calculate the wound area. We superimpose the leading edges on the experimental images in Fig. 2. The position of the detected edges suggests that the edge detection algorithm clearly and ac-

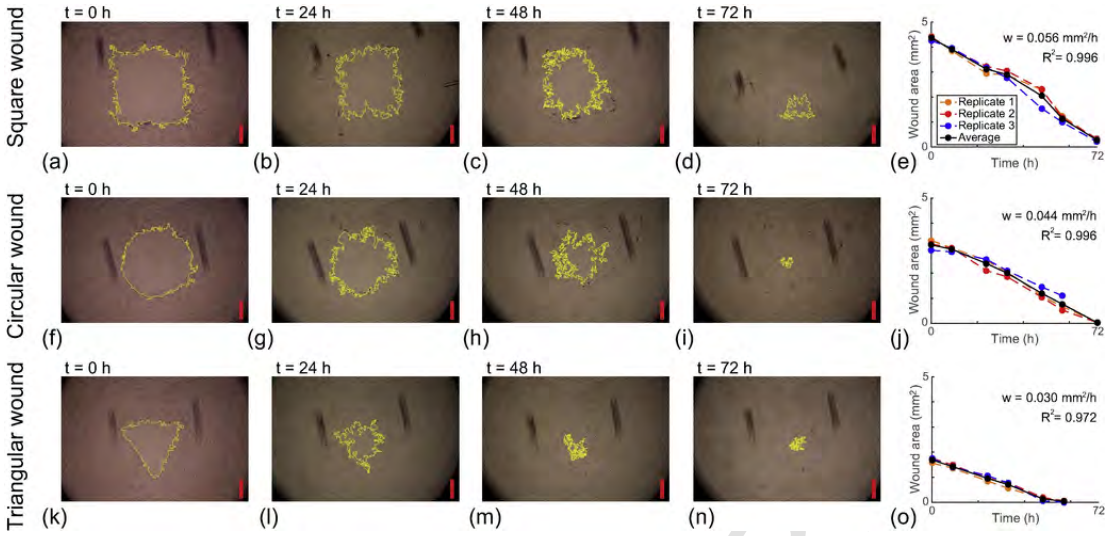

Fig. 2. Experimental images superimposed with the position of the leading edge. Images of wound healing assays at t = 0,24,48, and 72 h with initially (a)–(d) square, (f)–(i) circular, and (j)–(m) triangular wound shapes. The detected edges are shown in yellow. The scale bar corresponds to 500 μm. (e), (j), and (o) show the time evolution of the wound area for square, circular, and triangular wound shape, respectively. The rate of wound closure, w, and the coefficient of determination, R^2, are indicated.

curately detects the edge of the populations. Results in Fig. 2 compare the experimental images and the position of the detected leading edge for one of the experimental replicates only. Similar data for the remaining experimental replicates are given in the Supplementary Material document. Data in Fig. 2 allows us to quantify the progression of the experiments. We plot the time evolution of the wound area for each initial wound shape in Fig. 2(e), (d), and (n). Since the wound area decreases approximately linearly for all initial wound shapes, we fit a straight line to the averaged data. The rates of closure are w = 0.056,0.044, and 0.030 mm^2/h for the square, circular and triangular wounds, respectively.

This data suggests that the wound closure rates vary, and the square wound closes almost twice as fast as the triangular wound. Presenting data in this way is a standard approach, and we might have anticipated that since the only difference in the experiments is the initial wound shape we might see very little differences in the rate of wound closure. We hypothesise that this difference could have two possible explanations:

(1) Perhaps cells behave differently (i.e. have different rates of motility and/or proliferation) when they are subjected to different initial wound shapes;
(2) Perhaps the differences in wound closure rates occur directly as a result of the differences in initial wound shape, and there is no difference in the underlying behaviour of individual cells.

To make a distinction between these two potential explanations, we now calibrate the mathematical model to our experimental data to provide parameter estimates for each initial wound shape.

3.2. Estimating the cell proliferation rate and carrying capacity density

We count the number of cells in three identically-sized rectangular subregions in the cell proliferation assays. Using this data, we calibrate the solution of the logistic growth model to the cell density information in all three subregions (Supplementary Material) to estimate r and K. The quality of match between the solution of the logistic model and the experimental data is very good (Supplementary Material). Estimates of $\bar{r}$ and $\overline{K}$ for each subregion are summarised in Table 2. Since the variation in $\bar{r}$ and $\overline{K}$ between the three subregions is relatively small, we further average these estimates to give overall estimates of

Table 2
Estimates of $\bar{r}$,$\overline{K}$ and doubling time $t_d = \ln(2)/\bar{r}$, in three different subregions. All estimates are given to two significant figures.

Subregion	$\bar{r}$ (/h)	t_d (h)	$\overline{K}$ (cells/μm^2)	$E_{\min}$ ((cells/μm^2)^2)
Yellow	0.030	23	1.4×10^{-3}	8.7×10^{-8}
Red	0.046	15	1.3×10^{-3}	1.2×10^{-7}
Blue	0.031	22	1.5×10^{-3}	9.4×10^{-8}
Mean ± Standard deviation	0.036 ± 0.009	19 ± 4	$1.4 \pm 0.07 \times 10^{-3}$	–

r = 0.036/h and $K = 1.4 \times 10^{-3}$ cells/μm^2. These estimates of r and K are similar to previously-reported estimates for fibroblast cells in different assays (Simpson et al., 2013; Treloar et al., 2014).

3.3. Estimating the cell diffusivity

We now apply the discrete model to mimic the sticker assays to estimate D. Our estimate of r in Section 3.2 allows us to specify the ratio P_p/τ. If we take τ = 0.05 h and P_p = 0.0018, then the proliferation rate is $r = P_p/\tau$ = 0.036/h. To estimate D, we consider the diffusivity parameter to lie within the interval, 500?D?2000 μm^2/h (Johnston et al., 2016; Simpson et al., 2013). For our choice of Δ and τ, this interval of D corresponds to 0.16?P_m?0.64, and we seek to find a value of P_m, and hence D, which provides the best match between the discrete model and the experimental images for each wound shape. Our estimates of $\overline{D}$ are summarised in Table 3. Additional simulation and calibration results are presented and discussed in the Supplementary Material. There are two notable features of our estimates: (1) The difference between the average $\overline{D}$ for the three wound shapes is relatively small; and (2) the range of estimated $\overline{D}$ for the three wound shapes overlap. Therefore, the simplest explanation of our model calibration procedure is that our estimates of D are effectively independent of the initial wound shape. Therefore, if we pool these estimates and work with two significant figures, our overall estimate of the cell diffusivity

Table 3
Estimates of $\overline{D}$. All parameter estimates are given to two significant figures.

Square wound shape	$\overline{D}$ (μm²/h)	E_{min} (mm⁴)
Experimental replicate 1	1200	8.6×10^{-2}
Experimental replicate 2	1000	8.4×10^{-2}
Experimental replicate 3	1400	1.5×10^{-2}
Mean ± Standard deviation	1200 ± 200	–
Circular wound shape	$\overline{D}$ (μm²/h)	E_{min} (mm⁴)
Experimental replicate 1	1000	3.3×10^{-2}
Experimental replicate 2	1300	1.0×10^{-2}
Experimental replicate 3	700	1.3×10^{-2}
Mean ± Standard deviation	1000 ± 300	–
Triangular wound shape	$\overline{D}$ (μm²/h)	E_{min} (mm⁴)
Experimental replicate 1	1500	8.0×10^{-3}
Experimental replicate 2	1000	1.2×10^{-2}
Experimental replicate 3	1400	2.8×10^{-2}
Mean ± Standard deviation	1300 ± 270	–

is 1200 ± 260 μm²/h, which is consistent with previous values obtained in other assays (Simpson et al., 2013; Treloar et al., 2014).

To provide an additional check on the ability of our mathematical model to predict the experiments, we now explore how well the solution of Eq. (1), with $r = 0.036$/h, $K = 1.4 \times 10^{-3}$ cells/μm², and $D = 1200$ μm²/h, provides a useful prediction of the experimental data. To do this we solve Eq. (1) on the same domain as we use in our previous discrete simulations, with zero net flux (symmetry) boundary condition on all boundaries. The initial condition is $\mathscr{C}(x,y,0) = 0$ in the initial wound area, and $\mathscr{C}(x,y,0) = 0.4K$ elsewhere. Using the method of lines, Eq. (1) is discretised with a central difference approximation with uniform node spacing, δ (Supplementary Material). The resulting system of ODEs is solved using the MATLAB function *ode45*, with tolerance *?* (MathWorks, 2017). We superimpose the numerical solution of Eq. (1) on the experimental images by showing the contour, $\mathscr{C}(x,y,t) = 0.2K$, at various times. This choice of contour provides a good estimate of the density at the leading edge detected by ImageJ (Supplementary Material). Comparing the solution of Eq. (1) presented in terms of the contour of the leading edge density and the experimental images suggests that our mathematical model, parameterised with a unique combination of parameters, predicts the time evolution of the wound area for all three initial wound shapes (see Fig. 3).

4. Conclusions

Previous experimental studies describe wound healing assays by reporting the time evolution of wound area. When we report the results from our sticker assays in this standard way, we find that the area of the circular, square and triangular wounds close linearly with time. However, the rate of closure is very different between the three initial wound shapes. Without further examination, this standard data might suggest that the mechanisms driving wound closure could depend, somehow, on the initial wound shape. To provide further information, we quantify the relevant mechanisms in the experiments by calibrating the solution of a discrete random walk model, and the continuum-limit description of this model, to the experimental data. In summary, we find that our parameter estimates for each initial wound shape are similar. Therefore, the simplest possible explanation of our results is that the solution of the mathematical model with a unique choice of parameters provides a good match of the experimental data. Therefore, while the temporal wound area data depends on the initial wound shape, the underlying mechanisms that drive the behaviour of the cell populations do not depend on the initial wound shape.

Uncited reference

Jonkman et al. (2014).

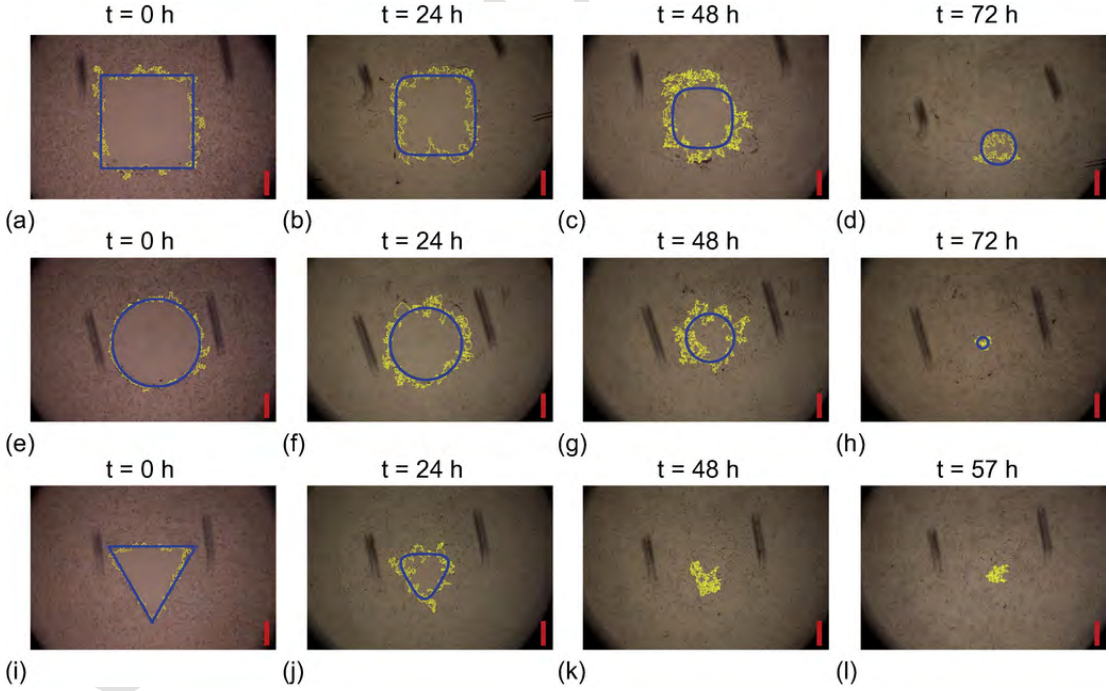

Fig. 3. Contour plot of numerical solutions of Eq. (1) for the sticker assays. The wound closure with initially square, circular and triangular wound shapes are shown in (a)–(d), (e)–(h), and (i)–(l), respectively. The blue contour plot that corresponds to $\mathscr{C}(x,y,t) = 0.2K$ is superimposed onto the detected edge in each subfigure. The scale bar corresponds to 500 μm. The numerical solutions of Eq. (1) is obtained with $D = 1200$ μm²/h, $r = 0.036$/h, $K = 1.4 \times 10^{-3}$ cells/ μ m², $\delta = 10$ μm, and $? = 1 \times 10^{-5}$. (For interpretation of the references to colour in this figure legend, the reader is referred to the web version of this article.)

Acknowledgments

We are supported by the Australian Research Council (DP140100249, DP170100474) and the Taiwan Ministry of Science and Technology (MOST 106-2313-B-002-031-MY3). Wang Jin is supported by a QUT Vice Chancellor's Research Fellowship. We appreciate the comments from two reviewers.

Appendix A. Supplementary material

Supplementary data associated with this article can be found, in the online version, at https://doi.org/10.1016/j.ces.2018.01.004.

References

Ariano, P., Dalmazzo, S., Owsianik, G., Nilius, B., Lovisolo, D., 2011. TRPC channels are involved in calcium-dependent migration and proliferation in immortalized GnRH neurons. Cell Calcium 49, 387–394.

Ascione, F., Caserta, S., Guido, S., 2017. The wound healing assay revisited: a transport phenomena approach. Chem. Eng. Sci. 160, 200–209.

Bachstetter, A.D., Zhou, Z., Rowe, R.K., Xing, B., Goulding, D.S., Conley, A.N., Sompol, P., Meier, S., Abisambra, J.F., Lifshitz, J., Watterson, D.M., 2016. MW151 inhibited IL–1β levels after traumatic brain injury with no effect on microglia physiological responses. PLOS One 11, e0149451.

Fisher, R.A., 1937. The wave of advance of advantageous genes. Ann Eugen 7, 353–369.

Gough, W., Hulkower, K., Lynch, R., Mcglynn, P., Uhlik, M., Yan, L., Lee, J., 2011. A quantitative, facile, and high–throughput image–based cell migration methods is a robust alternative to the scratch assay. J. Biomol. Screen. 16, 155–163.

Jin, W., Shah, E.T., Penington, C.J., McCue, S.W., Chopin, L.K., Simpson, M.J., 2016. Reproducibility of scratch assays is affected by the initial degree of confluence: experiments, modelling and model selection. J. Theor. Biol. 390, 136–145.

Jin, W., Penington, C.J., McCue, S.W., Simpson, M.J., 2016. Stochastic simulation tools and continuum models for describing two–dimensional collective cell spreading with universal growth functions. Phys. Biol. 13, 056003.

Johnston, S.T., Shah, E.T., Chopin, L.K., McElwain, D.L.S., Simpson, M.J., 2015. Estimating cell diffusivity and cell proliferation rate by interpreting IncuCyte ZOOM™ assay data using the Fisher–Kolmogorov model. BMC Syst. Biol. 9, 38.

Johnston, S.T., Ross, J.V., Binder, B.J., McElwain, D.L.S., Haridas, P., Simpson, M.J., 2016. Quantifying the effect of experimental design choices for in vitro scratch assays. J. Theor. Biol. 400, 19–31.

Jonkman, J.E., Cathcart, J.A., Xu, F., Bartolini, M.E., Amon, J.E., Stevens, K.M., Colarusso, P., 2014. An introduction to the wound healing assay using live–cell microscopy. Cell Adhes. Migr. 8, 440–451.

Katakowski, M., Zheng, X., Jiang, F., Rogers, T., Szalad, A., Chopp, M., 2010. MiR–146b–5p suppresses EGFR expression and reduces in vitro migration and invasion of glioma. Cancer Invest. 28, 1024–1030.

Keese, C.R., Wegener, J., Walker, S.R., Giaever, I., 2004. Electrical wound–healing assay for cells in vitro. Proc. Natl. Acad. Sci. USA 101, 1554–1559.

Kramer, N., Walzl, A., Unger, C., Rosner, M., Krupitza, G., Hengstschlger, M., Dolznig, H., 2013. In vitro cell migration and invasion assays. Mutat. Res. Rev. Mutat. Res. 752, 10–24.

Lee, J., Wang, Y.L., Ren, F., Lele, T.P., 2010. Stamp wound assay for studying coupled cell migration and cell debris clearance. Langmuir 26, 16672–16676.

Leu, J.G., Chen, S.A., Chen, H.M., Wu, W.M., Hung, C.F., Yao, Y.D., Tu, C.S., Liang, Y.J., 2012. The effects of gold nanoparticles in wound healing with antioxidant epigallocatechin gallate and α–lipoic acid. Nanomed. Nanotechnol. 8, 767–775.

Liang, C.C., Park, A.Y., Guan, J.L., 2007. In vitro scratch assay: a convenient and inexpensive method for analysis of cell migration in vitro. Nat. Protoc. 2, 329–333.

Madison, J.B., Gronwall, R.R., 1992. Influence of wound shape on wound contraction in horses. Am. J. Vet. Res. 53, 1575–1578.

Mamouni, J., Yang, L., 2011. Interdigitated microelectrode–based microchip for electrical impedance spectroscopic study of oral cancer cells. Biomed. Microdevices 13, 1075–1088.

MathWorks. Ode45. <https://au.mathworks.com/help/matlab/ref/ode45.html> (accessed: December 2017).

MathWorks. Lsqcurvefit. <https://au.mathworks.com/help/optim/ug/lsqcurvefit.html> (accessed: December 2017).

Riahi, R., Yang, Y., Zhang, D.D., Wong, P.K., 2012. Advances in wound–healing assays for probing collective cell migration. J. Lab. Autom. 17, 59–65.

Simpson, M.J., Landman, K.A., Hughes, B.D., 2010. Cell invasion with proliferation mechanisms motivated by time–lapse data. Physica A 389, 3779–3790.

Simpson, M.J., Treloar, K.K., Binder, B.J., Haridas, P., Manton, K.J., Leavesley, D.I., McElwain, D.L.S., Baker, R.E., 2013. Quantifying the roles of cell motility and cell proliferation in a circular barrier assay. J. R. Soc. Interface 10, 20130007.

Treloar, K.K., Simpson, M.J., 2013. Sensitivity of edge detection methods for quantifying cell migration assays. PLOS One 8, e67389.

Treloar, K.K., Simpson, M.J., McElwain, D.L.S., Baker, R.E., 2014. Are in vitro estimates of cell diffusivity and cell proliferation rate sensitive to assay geometry?. J. Theor. Biol. 356, 71–84.

Tremel, A., Cai, A., Tirtaatmadja, N., Hughes, B.D., Stevens, G.W., Landman, K.A., O'Connor, A.J., 2009. Cell migration and proliferation during monolayer formation and wound healing. Chem. Eng. Sci. 64, 247–253.

Ueck, C., Volksdorf, T., Houdek, P., Vidal-y-Sy, S., Sehner, S., Ellinger, B., Lobmann, R., Larena-Avellaneda, A., Reinshagen, K., Ridderbusch, I., Kohrmeyer, K., 2017. Comparison of in–vitro and ex–vivo wound healing assays for the investigation of diabetic wound healing and demonstration of a beneficial effect of a triterpene extract. PLOS One 12, e0169028.

van der Meer, A.D., Vermeul, K., Poot, A.A., Feijen, J., Vermes, I., 2010. A microfluidic wound–healing assay for quantifying endothelial cell migration. Am. J. Physiol.–Heart Circ. Physiol. 298, H719–H725.

Vedula, S.R., Ravasio, A., Lim, C.T., Ladoux, B., 2013. Collective cell migration: a mechanistic perspective. Physiology 28, 370–379.

Yarrow, J.C., Perlman, Z.E., Westwood, N.J., Mitchison, T.J., 2004. A high–throughput cell migration assay using scratch wound healing, a comparison of image–based readout methods. BMC Biotechnol 4, 21.